IEEE Access
Multidisciplinary | Rapid Review | Open Access Journal

Received January 6, 2019, accepted February 1, 2019, date of publication February 5, 2019, date of current version February 22, 2019.

Digital Object Identifier 10.1109/ACCESS.2019.2897740

Transverse Magneto-Optic Error of a Miniature Solid-Core Photonic-Crystal Fiber Optic Gyroscope

WEI CAI, NINGFANG SONG, JINGMING SONG, JING JIN, AND XIAXIAO WANG
School of Instrument Science and Opto-Electronic Engineering, Beihang University, Beijing 100191, China

Corresponding author: Wei Cai (sdfz174caiwei@126.com)

This work was supported in part by the National Natural Science Foundation of China under Grant 61575012 and Grant 61575013, in part by the National Key Scientific Instrument and Equipment Development Project under Grant 2013YQ040877, and in part by the Academic Excellence Foundation of BUAA for Ph.D. Students.

ABSTRACT The transverse magneto-optic error is a significant nonreciprocal error of fiber optic gyroscopes, particularly for the miniature fiber optic gyroscope. In this paper, the transverse magneto-optic error of a solid-core photonic-crystal fiber optic gyroscope is theoretically analyzed and experimentally measured, as well as compared with that of the conventional fiber optic gyroscopes. The results show that the transverse magneto-optic error per turn of the miniature photonic-crystal fiber optic gyroscope is ~ 3.5 times smaller than that of the conventional fiber optic gyroscopes. A thinner μ-metal shield can be used in a miniature photonic-crystal fiber optic gyroscope, resulting in less cost and weight. Meanwhile, the experimental and the calculated results agree well with each other, which illustrates that the transverse magneto-optic error derives mainly from the bend-induced asymmetry distribution of the refractive index in fiber. Considering the remarkable properties of the solid-core photonic-crystal fibers, they are the good candidates for the future miniature fiber optic gyroscopes.

INDEX TERMS Gyroscopes, optical fiber sensors, optical fibers.

I. INTRODUCTION

The fiber optic gyroscope (FOG) is one of the most successful fiber sensors [1] and is a key component of inertial navigation systems. Magnetic shields are widely used to reduce the magnetic-field dependence of FOGs [2]–[6]. However, this method increases the dimension and weight of FOGs. The dimension and weight requirements of inertial navigation systems have become tighter over the past few years, particularly for micro-satellites. Photonic-crystal fibers (PCFs) offer a new means to solve this problem. Polarization-maintaining solid-core PCFs based on shape birefringence have fewer spurious twist per unit length than conventional polarization-maintaining fibers (PMFs) based on a stress structure. The magnetic-field-induced Faraday nonreciprocal error of PCF-FOGs is about ten times lower than that of a PMF-FOG [5], which makes the solid-core PCF promising for the miniature FOGs.

The associate editor coordinating the review of this manuscript and approving it for publication was Kin Kee Chow.

Another kind of magnetic-field-induced nonreciprocal error in FOGs is the transverse magneto-optic error (TMOE) induced by a magnetic field component orthogonal to fiber. The TMOE of FOGs was first analyzed by Logozinskii [6], who showed that the TMOE is proportional to the number of turns in the coil. The TMOE originates from a magnetically induced lateral shift of the fiber mode [6]. Zhang *et al.* [7] found that the TMOE in PMF-FOGs is not only curve-radius related, but it is also related to the polarization state of the light, errors in coupling angles between the pigtails of multi-function integrated optic circuit and the PMF coil, the pressure in fiber coil, and the twist rate of the fiber [8]. The Faraday nonreciprocal error grows as the square root of the length of the coil [3], whereas the TMOE is proportional to the number of turns in the coil, i.e., the ratio of the length over the diameter of the coil [6]. Then, the ratio the TMOE over the Faraday error varies as the square root of the length over the diameter and becomes higher with small diameter coils. Thus, the TMOE is a significant factor of magnetically induced drift in FOGs, particularly for

the miniature FOGs. The magnetically induced lateral shift of the fiber mode is a micro perturbation of that induced by fiber bending. The solid-core PCF shows better bending characteristics than the conventional PMFs [9], [10]. Thus, the mode of a photonic-crystal fiber (PCF) may shift by a smaller amount than the mode of a conventional PMF. A PCF-FOG possibly shows less TMOE than a PMF-FOG under the same conditions.

In this paper, we studied the TMOE of the PCF-FOG for the first time, to the best of our knowledge. Theoretical analyses are given to describe the TMOE of FOGs. Moreover, the simulation and experimental results of the PCF-FOG and the conventional PMF-FOG are comparatively illustrated. The experimental and simulation results agree well with each other, which indicates that the TMOE is related to the bend-induced asymmetry distribution of the refractive index in fiber. The results show that the PCF-FOG has ~ 3.5 times smaller TMOE per turn than the conventional PMF-FOG. Finally, the methods to further reduce the TMOE of the miniature FOGs are discussed.

II. THEORY AND ANALYSIS

An axial magnetic-field vector B_A can be decomposed into a component $B_{//}$ that is parallel to the fiber and a component $B_\perp$ that is orthogonal to the fiber as Fig.1 shows. The magnetic-induced nonreciprocal error can be divided into two parts. The first part is the Faraday error induced by the magnetic component $B_{//}$, and the second part is the TMOE induced by the magnetic component $B_\perp$. Because the winding angle α in each layer is small enough and negligible, the magnetic component $B_{//}$ is negligible as well. The B_A is nearly perpendicular to the propagation direction of the optical waves. Thus, the TMOE is usually obtained by measuring the axial magnetic-field sensitivity of FOGs [6]–[8].

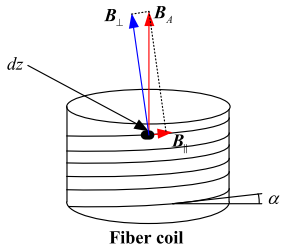

FIGURE 1. Decomposition of an axial magnetic-field vector B_A, which is nearly perpendicular to the propagation direction of the optical waves, because the winding angle α in each layer is negligible.

For the polarization maintaining fibers, there are usually two orthogonal axes, which correspond to two polarized modes: the fast axis mode and the slow axis mode. We suppose that x is the direction perpendicular to the sensitive axis of the FOG, y is the direction parallel to the sensitive axis, z is the direction along the propagation of the optical waves, and θ (z) is the angle between the x-axis and the fast axis at position z as Fig. 2 shows. As it is done by Logozinskii [6], that the mode in a single mode fiber does not have a perfectly

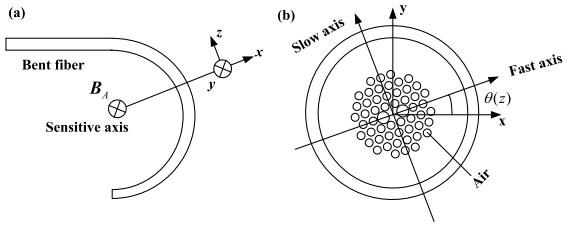

FIGURE 2. Coordinate of the bent fiber in the coil. (a) x is the direction perpendicular to the sensitive axis of the FOG; y is the direction parallel to the sensitive axis; z is the direction along the propagation of the optical waves. (b) θ (z) is the angle between the x-axis and the fast axis at position z.

transverse polarization. It has to be taken into account that it is a hybrid mode (HE) with a small longitudinal E_z component in addition to the E_x and E_y transverse components. The electromagnetic field vector on the x-axis and the y-axis can be expressed as:

$$\begin{cases} \left(e_f \cos(\theta), e_f \sin(\theta), e_z, -h_s \sin(\theta), h_s \cos(\theta), h_z\right) \\ \left(-e_s \sin(\theta), e_s \cos(\theta), e_z, -h_f \cos(\theta), -h_f \sin(\theta), h_z\right), \end{cases} \tag{1}$$

where $e_f, e_s e_z, h_f, h_s$, and h_z represent the electric-field vector and the magnetic-field vector along the fast axis, the slow axis, and the z-direction, respectively.

In the presence of a y-direction magnetic-field B_A, as shown in Fig. 2, the tensor matrix of the dielectric constant changes to [11]:

$$\varepsilon = \begin{vmatrix} n_x^2 & & i\delta \\ & n_y^2 & \\ -i\delta & & n_z^2 \end{vmatrix}, \tag{2}$$

where $\delta = \lambda V B_A n/\pi$; λ is the operating wavelength; V is the Verdet constant; n is the refractive index, which is approximate to the effective mode index of the fundamental mode. The fiber in the magnetic field is a slight perturbation of the original fiber, and the propagation constant of a mode with perturbations can be expressed as [12]:

$$\beta = \bar{\beta} + k \left(\frac{\varepsilon_0}{\mu_0}\right)^{\frac{1}{2}} \frac{\int_{A_\infty} \left(n^2 - \bar{n}^2\right) e \cdot \bar{e}^* dA}{\int_{A_\infty} \left(e \times \bar{h}^* + \bar{e}^* \times h\right) \cdot \hat{z} dA}, \tag{3}$$

where $\bar{\beta}$, $\bar{e}$, $\bar{h}$ are the propagation constant, the electric-field vector, and the magnetic-field vector of the mode without perturbations, respectively. $\bar{n}$ and n are the refractive index profile of the unperturbed and perturbed fibers, respectively. ε_0 and μ_0 are free-space dielectric constant and permeability. k is the free-space wave number, and $*$ denotes complex conjugate. A_∞ is the infinite cross-section, and the $\hat{z}$ is the unit vector parallel to the fiber axis.

For a sufficiently small perturbation, we can simplify (3) by assuming $e \cong \bar{e}$ and $h \cong \bar{h}$ as:

$$\beta = \bar{\beta} + \frac{\omega}{2} \frac{\int_{A_\infty} (\Delta\varepsilon \bar{e}) \cdot \bar{e}^* dA}{\int_{A_\infty} \left(\bar{e} \times \bar{h}^*\right) \cdot \hat{z} dA}, \tag{4}$$

where ω is the angular frequency of the optical wave. We can write propagation constants of the clockwise and the counter-clockwise modes as [7]:

$$\begin{cases} \beta_{F-CW} = \bar{\beta}_F + \delta\beta \\ \beta_{S-CW} = \bar{\beta}_S + \delta\beta' \\ \beta_{F-CCW} = \bar{\beta}_F - \delta\beta \\ \beta_{S-CCW} = \bar{\beta}_S - \delta\beta', \end{cases} \tag{5}$$

where $\bar{\beta}_F$ and $\bar{\beta}_S$ are propagation constants of the fast axis mode and the slow axis mode without perturbations, respectively.

When the fusion splicing angles between the pigtails of the MIOC and the fiber coil are both 0^o as Fig. 3 shows, the light is guided into the fast axis. The fiber coil can be divided into m segments, and the length of each segment is dz. The orientation of the polarization maintaining axis in each segment is unchanged. The total TMOE can be calculated by adding the TMOE of each segment. We assume that the bending radius of the fiber in different layers of the fiber coil is a constant. Considering $e_z = -\left(i/\beta\right)\left(\partial e_x/\partial x\right)$ and $h_y = \omega\varepsilon e_x/\beta$ when $\theta = 0^o$, the TMOE of the clockwise and the counter-clockwise optical waves can be deduced as [8]:

$$\begin{cases} \Delta\varphi = 2\delta\beta L = \dfrac{\lambda V B_A |\chi|}{\pi n} \sum\limits_{i=1}^{m} \cos^2\theta(i) dz \\ \chi = \dfrac{\iint \frac{\partial |e_x|^2}{\partial x} dxdy}{\iint |e_x|^2 \, dxdy}, \end{cases} \tag{6}$$

where χ is an asymmetry degree related to the bending radius of the fiber coil. e_x is the electric field vector along the x-direction when $\theta = 0^o$. The summation term in $\Delta\varphi$ corresponds to the twist in the fiber coil.

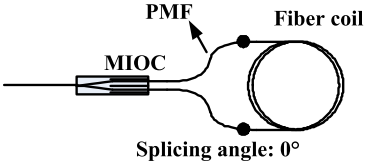

FIGURE 3. Splicing points between the pigtails of a multifunction integrated optic circuit (MIOC) and a fiber coil.

Due to the random twisting of the fiber in a coil, we assume the angle θ (z) is stochastic uniform distributed. Therefore, each of its birefringent axes coincides with the x-axis along approximately half the fiber length [5], [6], [13]. The statistical TMOE is:

$$\langle \Delta\varphi \rangle = \frac{\lambda V B_A |\chi| L}{2\pi n}, \tag{7}$$

where L is the length of the fiber coil. The equivalent axial magnetic-induced rotation rate error of a FOG can be expressed as:

$$\Omega(^o/h) = \frac{\lambda^2 c V B_A |\chi|}{4\pi^2 n D} \cdot \frac{180 \times 3600}{\pi}, \tag{8}$$

where D is the effective diameter of the fiber coil.

Considering the Verdet constant is proportional to $1/\lambda^2$ [14], the (8) can be simplified as:

$$\Omega(^o/h) \approx 2.25 \frac{B_A |\chi|}{nD}. \tag{9}$$

When the fiber is straight, the refractive index distribution of the fiber is symmetrical about the yoz plane. $|e_x|^2$ is an even function. Meanwhile, $\partial |e_x|^2/\partial x$ is an odd function about the yoz plane. Therefore, χ is zero theoretically. The propagation constants of the clockwise and the counter-clockwise optical waves are equal under this circumstance.

When the fiber is wound as a fiber coil, the field distribution of the fast axis mode appears a marginal displacement to the outside and $\partial |e_x|^2/\partial x$ is not an odd function about the yoz plane anymore. If the axial magnetic-field component B_A exists, the propagation constants of the clockwise and the counter-clockwise optical waves are slightly different, which induces the TMOE of FOGs. The total phase error is accumulated along the fiber coil. Thus, a significant magnetic-induced drift may exist in miniature FOGs. From the above theoretical derivation, it is known that the TMOE originates from the bend-induced asymmetry distribution of the refractive index in the fiber about the yoz plane.

III. NUMERICAL SIMULATION

In this section, we develop a theoretical model using the commercial software COMSOL Multiphysics 4.4 based on the full vector finite element method to precisely evaluate the TMOE of the PCF-FOG and the conventional PMF-FOG. Numerical simulations were conducted to investigate the value of the asymmetry degree χ with the perfect match layer (PML) boundary condition. The scanning electron micrographs of the PANDA fiber (PM1550B-80/135, FiberHome Telecommunication Technologies Co., Ltd.) and a kind of small diameter PM-PCF designed for miniature FOGs (FiberHome Telecommunication Technologies Co., Ltd.) [15] are shown in Fig. 4.

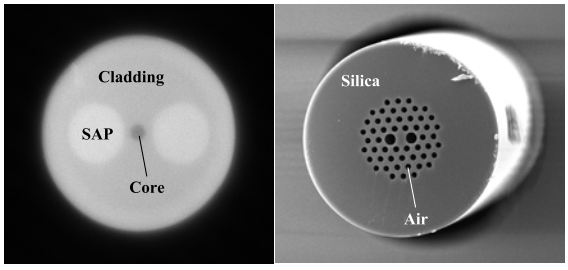

FIGURE 4. Cross-sections of the PANDA fiber and the small diameter PM-PCF.

The geometry parameters of the PANDA fiber and the small diameter PM-PCF are listed in Tables 1. The material parameters of the PANDA fiber are obtained from [16]. The operating wavelength is 1550 nm. The refractive indices of pure silica and air in PCF are 1.45 and 1, respectively.

For a bent fiber, the refractive index distribution is no longer symmetrical about the yoz plane. We assume the x-axis

TABLE 1. Geometry parameters of the panda fiber and the PM-Pcf.

Types of PMF	PANDA fiber (PM1550B-80/135)	PM-PCF
Geometry Parameters	Core diameter = 6 μm SAP diameter = 23 μm $r_{core\text{-}SAP}$ = 18 μm Cladding diameter = 80 μm Coating diameter = 135 μm	Large hole diameter = 5.70 μm Small hole diameter = 3.12 μm Pitch = 5.58 μm Cladding diameter =100μm Coating diameter =135μm

is defined to point towards the outside of the bend. The refractive index distribution of the silica becomes a function of the bending radius R_b as [17]:

$$n_{bend}(x, y) = n(x, y)\left(1 + \frac{x}{R_b}\right). \tag{10}$$

The mode patterns of the PANDA fiber and the small diameter PM-PCF for x polarizations are shown in Fig. 5, and the electric field directions are marked with red arrows.

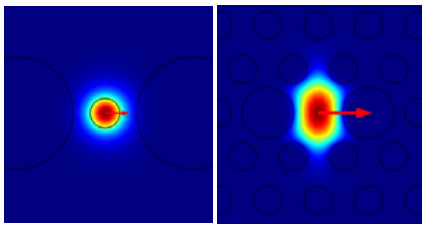

FIGURE 5. Field distributions of the PANDA fiber (left) and the small diameter PM-PCF (right) for x polarizations.

The normalized x-polarization electric field profiles of the straight PCF and the bent PCF are shown in Fig. 6. We can see that the electric field distribution is a quasi-Gaussian profile and $\chi \approx 0$ when the fiber is straight. When the fiber is bent with a bending radius of 17 mm, the electric field distribution is not symmetric about the fiber axis anymore and $|\chi| \approx 122/m$. The influence of the bending radius R_b on the asymmetry degree χ of the PANDA fiber and

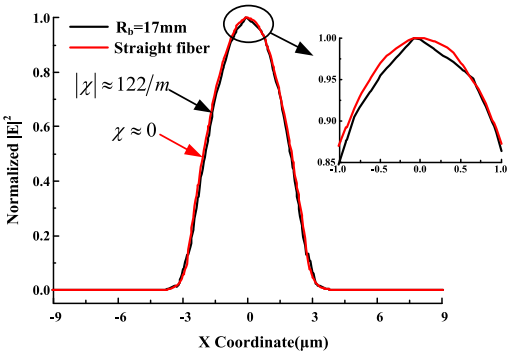

FIGURE 6. Normalized electric field profiles of the straight PCF (red line) and the bent PCF (black line) with a bending radius of 17 mm. The electric field distribution is a quasi-Gaussian profile when the fiber is straight, whereas it is not symmetric about the fiber axis when the fiber is bent.

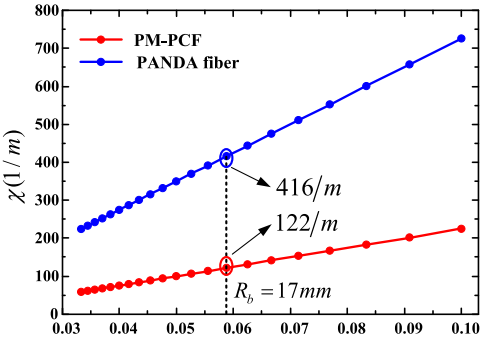

FIGURE 7. The asymmetry degree χ as a function of the bending radius.

the PM-PCF is also investigated and the results are shown in Fig. 7. We can see that the asymmetry degree increases as the bending radius decreases. The bending radius R_b varies from 10 mm to 30 mm, which almost covers FOGs from rate grade to intermediate grade.

The asymmetry degrees χ of the PM-PCF and the PANDA fiber when the bending radius is 17 mm are 122/m and 416/m, respectively. The effective fundamental mode index of the PM-PCF and PANDA fiber are 1.442 and 1.451, respectively. Considering $B_A = 10^{-4}$ T = 1 G and $D = 34$ mm, the calculated axial magnetic sensitivity of the miniature PCF-FOG and the conventional PMF-FOG according to (9) are 0.56°/(h·G) and 1.90°/(h·G), respectively.

IV. EXPERIMENT AND RESULT

Twelve fiber coils are quadrupole wound to measure the TMOE of FOGs. Six coils are made with the small diameter PM-PCF, meanwhile, the rest coils are made with the conventional PANDA fiber as Fig. 8 shows. All the coils are wound by the same person using the same winding machine and the same procedures. As the coating diameters of the PANDA fiber and the small diameter PM-PCF are both 135 μm. The dimension and the length of these coils are almost the same. The inner diameter of the coil is $\sim$ 26 mm, and the outer diameter is $\sim$ 39 mm. The effective diameter of these coils is $\sim$ 34 mm. The height of the coils is $\sim$ 9 mm, and the total length of the fiber coils is $\sim$ 300 m.

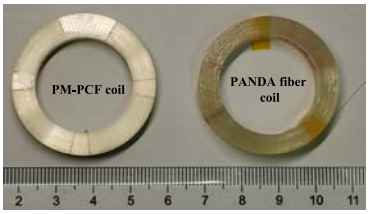

FIGURE 8. The fiber coils wound with the small diameter PM-PCF and the PANDA fiber.

Figure 9 presents a diagram of the FOG. An SLD light source with a spectral width of 45 nm, and $\pi/2$ modulation scheme is used in the test. The biased modulated signal is

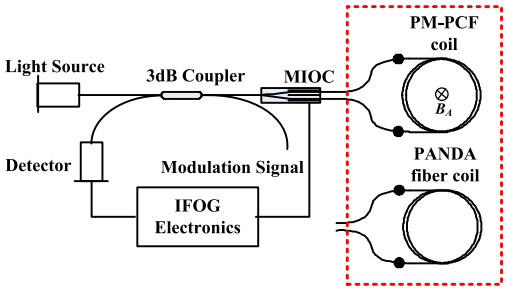

FIGURE 9. Schematic diagram of the FOG.

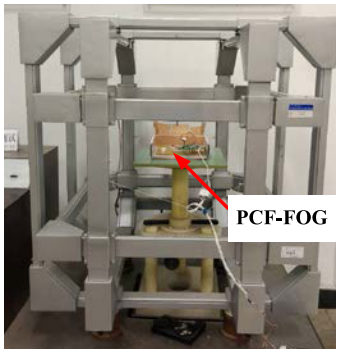

FIGURE 10. The test platform and the Helmholtz coil. The sensing axis of the fiber coil is perpendicular to the horizontal plane during the experiment and parallel to the magnetic field direction.

measured by demodulating the detector signal with a lock-in amplifier.

All the optical components were placed separately on a rotatable platform which is surrounded by a Helmholtz coil as Fig. 10 shows. The sensing direction of the fiber coil is perpendicular to the horizontal plane during the experiment. The sensing axis of the fiber coil is guaranteed parallel to the magnetic field by adjusting the platform carefully. The magnitude of the magnetic field was controlled by changing the driving current of the Helmholtz coil. The room temperature was maintained at around 25 ° C during the whole experiment.

The outputs of a PCF-FOG under different axial magnetic-field magnitudes are shown in Fig. 11 as an example, where 0 G means that only the Earth's magnetic-field exists. The output signal of the PCF-FOG at 0 G corresponds to a rotation rate of the FOG in Beijing, which is the reference for the measurement of the magnetic-induced bias. The integration time of the PCF-FOG is 1 s. The red dash lines represent the average outputs of the PCF-FOG within the 300-s test under the same magnetic-field magnitude. The measured magnetic sensitivity to the axial magnetic-field of the PM-PCF coils and the PANDA fiber coils are listed in Table 2.

The mean value and the standard deviation of the magnetic-induced bias of these coils under the same magnetic-field magnitude are shown in Fig. 12. We can see that the magnetic-induced bias of the conventional PMF-FOG and the PCF-FOG is proportional to the axial magnetic-field

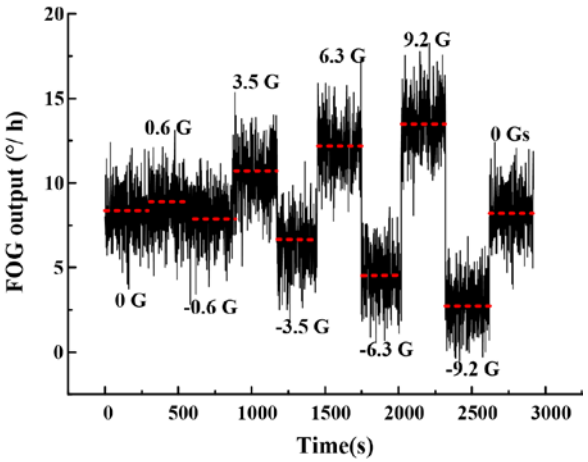

FIGURE 11. The output signal of the PCF-FOG recorded under different axial magnetic-field magnitudes at room temperature, where 0 G means that only the Earth's magnetic-field exists. The integration time of the PCF-FOG is 1 s.

TABLE 2. Magnetic sensitivity to the axial magnetic-field of the PCF coils and the panda fiber coils.

Types of the fiber coil	Calculated (°/(h·G))	Measured (°/(h·G))	
PM-PCF coil	0.56	No. 1	0.59
		No. 2	0.72
		No. 3	0.63
		No. 4	0.71
		No. 5	0.78
		No. 6	0.43
PANDA fiber coil	1.90	No. 1	2.65
		No. 2	2.16
		No. 3	1.90
		No. 4	2.37
		No. 5	2.08
		No. 6	2.43

magnitude. The slopes of the fitted lines represent the average axial magnetic sensitivity of the PCF-FOG and the PMF-FOG, which are $\sim$ 0.64 °/(h·G) and $\sim$ 2.24°/(h·G), respectively. The measured results are comparable to that of the theoretically calculated, which illustrates that the TMOE stems mainly from the bend-induced asymmetry distribution of the refractive index in fiber. The slight mismatch probably results from the twisting distribution which cannot be accurately evaluated.

V. DISCUSSION

The bend-induced asymmetry distribution of the refractive index in fiber plays a dominant role in the TMOE of the FOGs based on theoretical analysis, and that is validated by the experiment results. Though this asymmetry is weak, it still has a significant influence on FOGs after accumulating along the fiber coil. The average axial magnetic sensitivity of the miniature PCF-FOG is $\sim$ 3.5 times smaller than that of the conventional PANDA fiber coil with similar dimension.

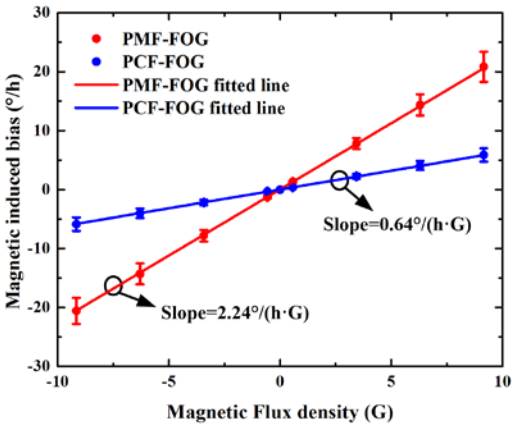

FIGURE 12. The output of the PCF-FOG and conventional PMF-FOG as a function of the axial magnetic-field magnitude.

The corresponding TMOE per turn of the PCF-FOG and the PMF-FOG are $\sim 1.5 \times 10^{-10} rad/(G \cdot turn)$ and $\sim 5.3 \times 10^{-10} rad/(G \cdot turn)$, respectively. The measured TMOE per turn of the conventional PMF-FOG is comparable to that analyzed in [6] and calculated in [13] ($4.0 \times 10^{-10} rad/(G \cdot turn)$). The lower axial magnetic sensitivity of PCF-FOG may be attributed to that the unique waveguiding properties of the solid-core PCF make it less sensitive to the bend-induced perturbations compared with the conventional PMFs based on a stress structure. However, the improvement is still not enough to build an inertial navigation system under harsh environments unless the PCF-FOG is equipped with a magnetic shield. The positive effect is that a thinner μ -metal shield can be used in the miniature PCF-FOG compared with the conventional PMF-FOG, resulting in reduced cost and weight.

A straightforward suggestion to further reduce the TMOE of miniature FOGs is to specially design the refractive index distribution of the fiber to compensate the bend-induced perturbation. However, the bend-induced perturbation can only be deducted when the fiber is wound with a specific orientation. This is challenging but is achievable if the outside coating layer is made into a partially flat shape for the convenience of winding a fiber coil. The approaches to realize a bend-compensated structure have been explored in [17]. The refractive index gradient can be achieved by stacking a few cells with different refractive index values, which is similar to the stack-and-draw method of PCF fabrication. Although the fabrication is challenging, this kind of bend-compensated fiber can offer robust bending characteristics.

For the solid-core PCF, it seems possible to further decrease the value of asymmetry degree by optimizing its structure parameters, because the properties of the solid-core PCF are closely related to its fiber structure. The change of structure parameters is similar to the change of refractive index distribution in the conventional fibers. In the next stage, we will investigate such structure parameters in order to further reduce the TMOE of PCF-FOGs. Another suggestion to eliminate this kind of bend-induced asymmetry is to substitute the solid-core PCF with the photonic-bandgap fiber. The optical wave is guided mainly in the air based on a resonance effect of the periodic partial reflections at the air-glass interfaces [18] in the photonic-bandgap fibers. Such a matter-free fiber is of great interest for the high-performance miniature gyroscopes because it drastically reduces matter-related effects such as the magneto-optic Faraday effect [5] and the bend-induced asymmetry distribution of refractive index. It is promising to remove the magnetic shield and further decrease the dimension and weight of the miniature FOGs based on the photonic-bandgap fiber. Although the present attenuation of the photonic-bandgap fiber is still on the order of several dB/km [19], it may be enough for miniature FOGs with a coil of two to three hundred meters in length. Further improvement is expected considering the recent progress.

VI. CONCLUSION

The TMOE of a solid-core photonic-crystal fiber optic gyroscope is theoretically analyzed and experimentally measured, as well as compared with that of the conventional PANDA fiber optic gyroscopes. The results indicate that the TMOE derives mainly from the bend-induced asymmetry distribution of the refractive index in fiber. The measured TMOE per turn of the miniature PCF-FOG is $\sim 1.5 \times 10^{-10} rad/(G \cdot turn)$, which is ~ 3.5 times smaller than that of the conventional PMF-FOGs ($\sim 5.3 \times 10^{-10} rad/(G \cdot turn)$). This result may be ascribed to the unique waveguiding properties of the solid-core PCF, which make the solid-core PCF less susceptible to the bend-induced perturbations than the PANDA fiber based on a stress structure. A thinner μ -metal shield can be used in a miniature PCF-FOG, which reduces the cost and weight. Solid-core PCFs are good candidates for future miniature FOGs considering its remarkable properties such as low bending loss, design flexibility, and less spurious twist per unit length.

ACKNOWLEDGMENT

The work was done at Beihang University. The authors would like to acknowledge all the staff in FiberHome Telecommunication Technologies Co., Ltd. for their technical feedback and support in the PCF fabrication.

REFERENCES

[1] H. K. Kim, M. J. F. Digonnet, and G. S. Kino, "Air-core photonic-bandgap fiber-optic gyroscope," *J. Lightw. Technol.*, vol. 24, no. 8, pp. 3169–3174, Aug. 2006.
[2] M. Digonnet, S. Blin, H. K. Kim, V. Dangui, and G. Kino, "Sensitivity and stability of an air-core fibre-optic gyroscope," *Meas. Sci. Technol.*, vol. 18, no. 10, pp. 3089–3097, Sep. 2007.
[3] K. Hotate and K. Tabe, "Drift of an optical fiber gyroscope caused by the Faraday effect: influence of the earth's magnetic field," *Appl. Opt.*, vol. 25, no. 7, pp. 1086–1092, Apr. 1986.
[4] T. Saida and K. Hotate, "General formula describing drift of interferometer fiber-optic gyro due to faraday effect: Reduction of the drift in twin-depo-I-FOG," *J. Lightw. Technol.*, vol. 17, no. 2, pp. 222–228, Feb. 1999.
[5] H. C. Lefevre, *The Fiber-Optic Gyroscope*, 2nd Ed. Norwood, MA, USA: Artech House, 2014.

[6] V. N. Logozinskii, "Magnetically induced non-faraday nonreciprocity in a fiber-optic gyroscope," *J. Commun. Technol. Electron.*, vol. 51, no. 7, pp. 836–840, Jul. 2006.
[7] D. W. Zhang, Z. F. Wang, L. Chen, X. Zhou, X. W. Shu, and C. Liu, "Nonreciprocity in single-mode fiber coil induced by orthogonal magnetic field," *J. Opt.*, vol. 15, no. 5, p. 6, May 2013.
[8] Y. X. Zhao *et al.*, "Nonreciprocal phase error caused by orthogonal magnetic field in a polarization-maintaining fiber-optic gyro," *IEEE Sensors J.*, vol. 15, no. 9, pp. 5128–5132, Sep. 2015.
[9] J. Tawney *et al.*, "Photonic crystal fiber IFOGs," in *Proc. Optical Fiber Sensors*, Cancún, Mexico, 2006, p. ME8.
[10] P. Russell, "Photonic crystal fibers," *Science*, vol. 299, no. 5605, pp. 358–362, 2003.
[11] P. Yeh and A. Yariv, "*Optical Waves in Crystals: Propagation and Control of Laser Radiation*. Hoboken, NJ, USA: Wiley, 1984.
[12] A. W. Snyder and J. Love, *Optical Waveguide Theory*. New York, NY, USA: Chapman & Hall, 1983.
[13] H. C. Lefèvre, "Potpourri of comments about the fiber optic gyro for its 40th anniversary, and how fascinating it was and it still is!" in *Proc. SPIE*, Baltimore, MD, USA, vol. 9852, 2016, Art. no. 985203.
[14] J. Noda, T. Hosaka, Y. Sasaki, and R. Ulrich, "Dispersion of Verdet constant in stress-birefringent silica fibre," *Electron. Lett.*, vol. 20, no. 22, pp. 906–908, Oct. 1984.
[15] N. Song, W. Cai, J. Song, J. Jin, and C. Wu, "Structure optimization of small-diameter polarization-maintaining photonic crystal fiber for mini coil of spaceborne miniature fiber-optic gyroscope," *Appl. Opt.*, vol. 54, no. 33, pp. 9831–9838, Nov. 2015.
[16] J. Song, K. Sun, S. Li, and W. Cai, "Phase sensitivity to temperature of the guiding mode in polarization-maintaining photonic crystal fiber," *Appl. Opt.*, vol. 54, no. 24, pp. 7330–7334, Aug. 2015.
[17] J. M. Fini, "Large mode area fibers with asymmetric bend compensation," *Opt. Express*, vol. 19, no. 22, pp. 21866–21873, Oct. 2011.
[18] R. F. Cregan *et al.*, "Single-mode photonic band gap guidance of light in air," *Science*, vol. 285, no. 5433, pp. 1537–1539, 1999.
[19] J. M. Fini *et al.*, "Polarization maintaining single-mode low-loss hollow-core fibres," *Nature Commun.*, vol. 5, p. 5085, Oct. 2014.

WEI CAI received the B.E. degree from Beihang University, Beijing, China, in 2012, where he is currently pursuing the Ph.D. degree. His current research interests include photonic-crystal fiber and fiber-optic gyroscope.

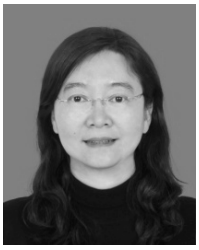

NINGFANG SONG received the B.E. degree from the Harbin Engineering University of China, Harbin, China, in 1989, and the M.E. and Ph.D. degrees from Beihang University, Beijing, China, in 1993 and 2004, respectively, where she is currently a Professor with the School of Instrument Science and Optic-Electronics Engineering. Her current research interests include fiber-optic gyroscope and inertial navigation systems.

JINGMING SONG received the B.E. and M.E. degrees from the Wuhan University of Technology of China, Wuhan, China, in 1996 and 2000, respectively, and the Ph.D. degree from the Huazhong University of Science and Technology, Wuhan, in 2005. He is currently an Associate Professor with the School of Instrument Science and Optic-Electronics Engineering, Beihang University, Beijing, China. His current research interest includes fiber sensors.

JING JIN was born in Inner Mongolia, China, in 1975. He received the Ph.D. degree in precision instrumentation and mechanism from Beihang University, Beijing, China, in 2008, where he is currently a Professor with the School of Instrument Science and Optic-Electronics Engineering. His main research interest includes optical sensors.

XIAXIAO WANG received the B.E., M.E., and Ph.D. degrees from Beihang University, Beijing, China, in 2000, 2002, and 2006, respectively, where he is currently an Associate Professor with the School of Instrument Science and Optic-Electronics Engineering. His current research interest includes fiber sensors.